

**An integrated dielectrophoresis-active hydrophoretic microchip for continuous particle filtration and separation**

Author

Yan, Sheng, Zhang, Jun, Pan, Chao, Yuan, Dan, Alici, Gursel, Du, Haiping, Zhu, Yonggang, Li, Weihua

Published

2015

Journal Title

Journal of Micromechanics and Microengineering

Version

Accepted Manuscript (AM)

DOI

[10.1088/0960-1317/25/8/084010](https://doi.org/10.1088/0960-1317/25/8/084010)

Rights statement

This is the Accepted Manuscript version of an article accepted for publication in Journal of Micromechanics and Microengineering. IOP Publishing Ltd is not responsible for any errors or omissions in this version of the manuscript or any version derived from it. The Version of Record is available online at <http://doi.org/10.1088/0960-1317/25/8/084010>

Downloaded from

<http://hdl.handle.net/10072/423799>

Griffith Research Online

<https://research-repository.griffith.edu.au>

# An integrated dielectrophoresis-active hydrophoretic microchip for continuous particle filtration and separation

Sheng Yan,<sup>1)</sup> Jun Zhang,<sup>1)</sup> Chao Pan,<sup>1)</sup> Dan Yuan,<sup>1)</sup> Gursel Alici,<sup>1,2)</sup> Haiping Du,<sup>3)</sup> Yonggang Zhu<sup>4,5,a)</sup> and Weihua Li<sup>1,a)</sup>

<sup>1</sup>*School of Mechanical, Materials and Mechatronic Engineering University of Wollongong, Wollongong, NSW 2522, Australia.*

<sup>2</sup>*ARC Centre of Excellence for Electromaterials Science, Innovation Campus, University of Wollongong, Wollongong, NSW 2500, Australia*

<sup>3</sup>*School of Electric, Computer and Telecommunication Engineering, University of Wollongong, Wollongong, NSW 2522, Australia*

<sup>4</sup>*CSIRO Manufacturing Flagship, Private Bag 10, Clayton South, VIC, 3169, Australia.*

<sup>5</sup>*Melbourne Centre for Nanofabrication/Australian National Fabrication Facility, 151 Wellington Road, Clayton, VIC, 3168, Australia*

<sup>a)</sup> Author to whom correspondence should be addressed. Electronic mail: weihuali@uow.edu.au and yonggang.zhu@csiro.au

Microfluidic manipulation of biological objects from mixture has a significant application in sample preparation and clinical diagnosis. This work presented a dielectrophoresis (DEP)-active hydrophoretic device for continuous label-free particle separation and filtration. This device comprises the interdigitated electrodes and a hydrophoretic channel. According to the difference of lateral positions of polystyrene particles, the device can run at separation or filtration modes by altering the power supply voltages. With an applied voltage of 24 V<sub>p-p</sub>, both 3 μm and 10 μm beads had close lateral positions and were redirected to the same outlet. Under a voltage of 36 V<sub>p-p</sub>, beads with the diameters of 3 μm and 10 μm had different lateral positions and be collected from the different outlets. Separation of 5 and 10 μm particles was achieved to demonstrate the relatively small size difference of the beads. This device has great potential in a range of lab-on-a-chip applications.

## 1 Introduction

The microfluidics has been witnessed significant developments in design, fabrication and experiments of lab-on-a-chip (LOC) platforms during the past decade <sup>1</sup>. As an interdisciplinary, this fascinating field of technology has found broad applications in sample preparation, clinical diagnosis, chemical analysis and electronics industries <sup>2, 3</sup>. One of the pivotal applications of microfluidics is to separate target cells from the mixture of biomedical samples based on their unique biophysical signatures <sup>4</sup>. Separation of biological objects is a primary step in preparative application such as point of care diagnosis.

Microfluidic techniques were divided into active and passive approaches according to the source of the manipulating force. Active manipulation utilises external energy such as acoustophoresis <sup>5</sup>, magnetophoresis <sup>6</sup> and dielectrophoresis(DEP) <sup>7-9</sup>, whereas passive methods utilise intrinsic hydrodynamic phenomena or the channel geometry such as pinched flow fractionation (PFF) <sup>10</sup>, deterministic lateral displacement (DLD) <sup>11, 12</sup>, hydrophoresis <sup>13-15</sup> and inertial microfluidics <sup>16-18</sup>. Typically, the active techniques have the capability to

precisely control the target particles and can be tuned in real-time, which allows the microfluidic devices more flexible and powerful. Due to its great potential DEP has made big progress in manipulating particles. Direct current (DC) DEP using electroosmosis flow to drive particles is pumpless method<sup>19</sup>. However, high voltage applied to the microfluidic device may generate Joule heat, not only resulting in the presence of bubbles, but also in a temperature distribution inside the channel. Also, the Joule heating phenomena is present in alternating current (AC) DEP, which employs AC signal to form non-uniform electric field. Beech *et al.*<sup>20</sup> proposed the arrays of insulator structures embedded in the channel for separation of polystyrene beads by the application of moderate ( $100 \text{ V cm}^{-1}$ ), low frequency (100 Hz) AC electric fields. Two-dimensional and three-dimensional microelectrodes were proposed for cell separation based on size differences or dielectric property<sup>21 22</sup>. Recently, a novel DEP-based approach was proposed by Song *et al.*<sup>23</sup>, who utilised on/off AC signal for sorting stem cells and their differentiation progeny. In the above approaches, the accurate control of sheath flow is a key factor that determined the separation performance as an inappropriate ratio of sheath flow and sample flow will deteriorate the separation efficiency. In comparison to the active approaches, a passive microfluidic platform is always easy and reliable to manipulate particles using the specific channel structures and sheath flows. Though the passive micro-channel can be easily parallelised, the fixed geometry and design of passive devices limit their operation range. Therefore, hybrid techniques are emerging to fill this gap, which take advantage of the merits of both active and passive methods.

Endeavours to employ external fields to passive techniques have been developed in the past. Wu *et al.*<sup>24</sup> reported a tunable PFF, which combined PFF and electroosmotic flow to tune the size separation of particles and separate *E. coli* and yeast cells. The combination of DEP and DLD was implemented by Beech *et al.*<sup>20</sup> to improve the sorting efficiency. This combined technique could not only separate particles with regards to size, it could also polarise them. Another impressive work was proposed by Zhang *et al.*<sup>3</sup> who successfully coupled DEP with inertial focusing. The focusing patterns and positions of the particles can be continuously adjusted by electric field in a high-throughput manner. Yan *et al.*<sup>25</sup> combined DEP with hydrophoresis to make hydrophoretic devices more tunable and flexible. Later, this technique was demonstrated to isolate plasma from whole blood and separate particles with regards to their sizes and dielectric properties<sup>26,27</sup>. Here, based on our previous work<sup>25-27</sup>, the further work is done to enable the DEP-active hydrophoretic device achieve dual-function (*e. g.* filtration and separation) in a single chip.

The main objective of the current study is to develop an integrated microfluidic device combining hydrophoresis and DEP for particle separation and filtration. Two modes, *i.e.*, filtration and separation modes, will be implemented in a single chip and can be switched by changing the voltages. The merits of the present effort lie in avoiding clogging and membrane-free. Compared to the conventional dead-end filtration, where the fluid direction is typically perpendicular to the filtration structure<sup>28, 29</sup>, the flow direction in our current device is parallel to the filtration microposts. Therefore, the problem of jamming is avoided. Cross-flow filtration suffers from membrane fouling, which limits the device to one-single use due to the sterility issue in most biological applications<sup>30,31</sup>. The membrane-free property of our technique allows repetitive use, which is cost-effective for many applications.

Additionally, the micro-posts involved in the microchannel serve as a repurifying unit, which further improve the separation efficiency compared to our prior research<sup>27</sup>.

The remainder of this paper is organized as follows. Section 2 will introduce material and methods including methodology, modelling, and experimental details. The main results will be presented in Section 3 which include particle filtration and separation based on the external electric field. The main conclusions will be drawn in Section 4.

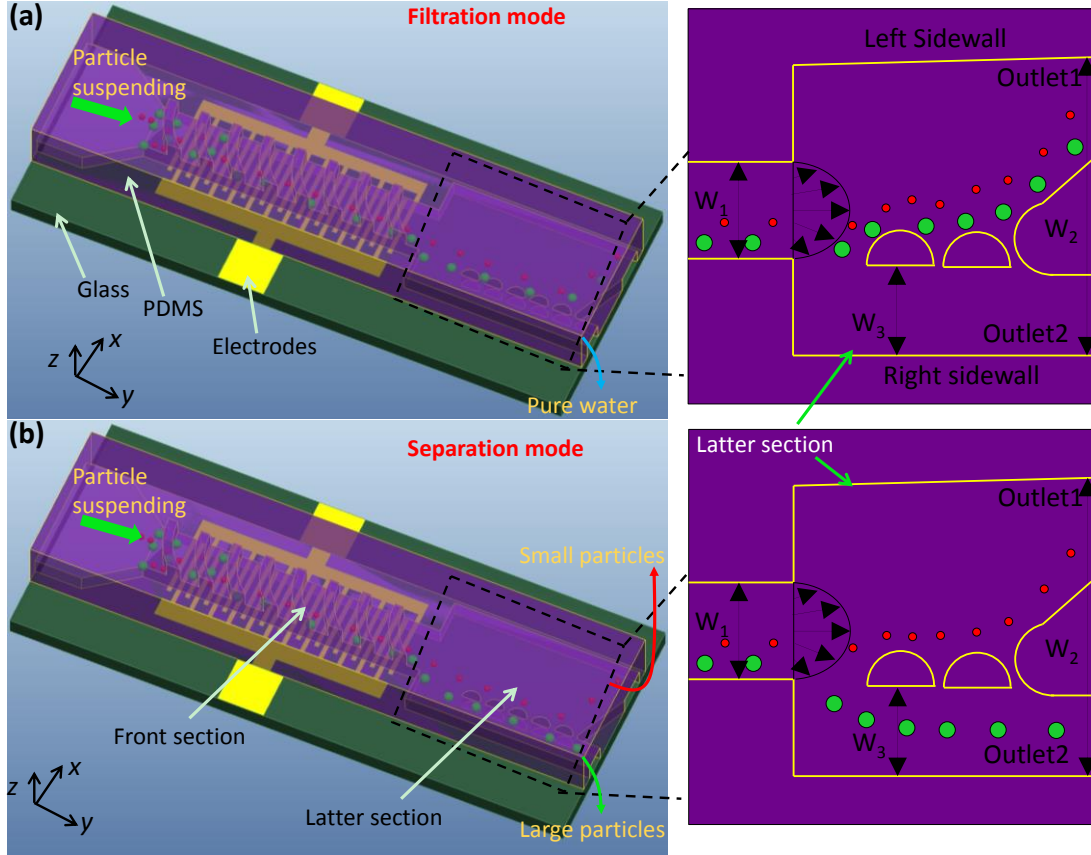


Figure 1 (a) The schematic of DEP-active hydrophoretic device for particle filtration. The microchip consists of a PDMS slab with micro-channel and a glass slide with interdigitated electrodes. Both large and small particles can be focused onto the right sidewall under external electric field in the front section of the channel. After entering the latter section, all beads cannot pass through the gap between micro-posts and right sidewall under the low voltage and therefore purified water can be collected from the Outlet 2 (right inset). (b) An overview of DEP-active hydrophoretic device for particle separation. Small and large particles can be separated by the microposts embedded in the micro-channel at the high voltage. Particles with the diameters of 3  $\mu\text{m}$  and 10  $\mu\text{m}$  are collected from the different outlets (right inset).

## 2 Material and methods

### 2.1 Methodology

The time-average of DEP force  $\mathbf{F}_{\text{DEP}}$ , are given by<sup>32</sup>:

$$\mathbf{F}_{\text{DEP}} = 2\pi\epsilon_m r^3 \text{Re}[K(\omega)]\nabla E^2 \quad (1)$$

where  $\epsilon_m$  is the absolute permittivity of the suspending medium, and  $r$  donates the particle radius,  $\nabla E^2$  is the gradient of the square of the applied field  $E$ ,  $\text{Re}$  indicates the real part.  $K(\omega)$  refers to the Clausius-Mossotti (CM) factor which depends on the complex

permittivities of the particle and the suspending medium, and the frequency of the external electric field as well:

$$K(\omega) = \frac{\varepsilon_p^* - \varepsilon_m^*}{\varepsilon_p^* + 2\varepsilon_m^*} \quad (2)$$

where  $\varepsilon^* = \varepsilon - i\sigma/\omega$  ( $i^2 = -1$ ) is the complex permittivities,  $\sigma$  is the electrical conductivity, and  $\omega$  is the frequency of the electric field. The subscripts ( $p, m$ ) represents the particle and suspending medium, respectively. The  $K(\omega)$  factor, a dominating role in DEP force, represents the dielectric properties of particles and suspending medium under different frequencies of the electric field applied. If the permittivity of a particle is greater than that of the suspending medium ( $K(\omega) > 0$ ), a positive DEP is generated in this mode, where the particle migrates to the region of a strong electric field. However, if  $K(\omega) < 0$ , the motion of the particle is repelled from the region of a strong electric field, which is termed negative DEP.

According to the equation (1), the DEP force relies on the square of the applied field, which implies that the larger the electric field applied, the greater DEP force will act on the particles. Also, the CM factor is a key parameter, which is ranging from -0.5 to 1. According to the previous work of Park *et al*<sup>21</sup>, the  $K(\omega)$  of polystyrene particles is -0.5 at a frequency of 1MHz, which means particles will exert maximum negative DEP force. Additionally, the DEP force is related to the particle size.

Hydrophoresis utilises a steric hindrance mechanism to separate or focus particles under a pressure gradient induced by anisotropic flow resistance<sup>33</sup>. Particles suspended in the medium will follow the rotational flows. When a particle is comparable in size with the height of the channel ( $h$ ), the particle motion depends on a kind of steric hindrance mechanism, which deflects the particles from their streams and lead to a new equilibrium position called hydrophoretic ordering<sup>34</sup>. The hydrophoretic equilibrium position ( $L_p$ ) depends on the following dimensionless parameters as experimentally studied<sup>35</sup>:

$$L_p \propto f\left(\frac{w}{d}, \frac{h}{d} \text{Re}\right) \quad (3)$$

where  $w$  is the channel width and  $d$  is the diameter of the particle. Re is the Reynolds number which is defined as  $\text{Re} = \rho u L / \mu$  where  $L$  is a characteristic linear dimension of the fluidic channel,  $u$  is the velocity of the liquid,  $\mu$  is its viscosity, and  $\rho$  is its density. A particle satisfying  $h \leq 2d$  can focus to an equilibrium position<sup>36</sup>. A particle, however, with the diameter less than the half of the channel height will follow the rotational flows generated by microgrooves and move back and forth in the channel.

In this DEP-active hydrophoretic device, although the real channel height cannot be change any longer, the position of a particle in the height direction can be tuned by exerting negative DEP force. Increasing the electric field will levitate particles to higher positions in the channel, which is equivalently treated as reducing the channel height. In such circumstance the small particle unsatisfying  $h \leq 2d$  can still focus to an equilibrium position under the appropriate applied voltage.

This DEP-active hydrophoretic microchip consists of a polydimethylsiloxane (PDMS) slab with micro-channel and a glass slide with interdigitated electrodes. The front section of the micro-device is a DEP-active hydrophoretic focuser for particle focusing, while the latter section is for particle filtration or separation (Fig. 1). In the front section, interdigitated electrodes were patterned onto the bottom of the channel so that particles exerting a negative DEP force were pushed into a narrow space. As a result, particles formed the hydrophoretic ordering would have an equivalent path in the front part and remain along the right sidewall.

Once entering the latter section of the channel, the large particles with 10  $\mu\text{m}$  in diameter will go through the gap between micro-posts and the right sidewall at the relatively high voltage ( $36 V_{p-p}$ ) in the separation mode (Fig. 1b), whereas they will not at the relatively low voltage ( $24 V_{p-p}$ ) in the filtration mode (Fig. 1a). For 3  $\mu\text{m}$  beads, they are unable to pass through the gap under any voltage applied in this experiment. Therefore, there are two different working modes based on different voltages. The first mode, called filtration mode, is that both 3  $\mu\text{m}$  and 10  $\mu\text{m}$  particles cannot pass through the gap under the low voltage and therefore purified water can be collected from the Outlet 2 (Fig. 1a). In another mode named separation mode, 3  $\mu\text{m}$  and 10  $\mu\text{m}$  particles can be separated by the microposts embedded in the micro-channel at the high voltage (Fig. 1b). Finally, 3  $\mu\text{m}$  and 10  $\mu\text{m}$  particles are collected from the different outlets (Fig. 1b). The series of microposts serve as pressure shunts to balance the pressure between Outlet 1 and Outlet 2. Additionally, 10  $\mu\text{m}$  particles are larger than the minimum space between neighbouring microposts (8  $\mu\text{m}$ ), indicating that large particles will not pass the microposts, which improves the separation efficiency. This passive method is simple, reliable and avoids any disturbances from downstream in the device, such as removal and insertion of tubes for collection<sup>37</sup>.

## 2.2 Modelling

In order to better understand the movements of particles, a commercial multiphysics modeling software package COMSOL was used to calculate the particle trajectories (Fig. 2). The modeling details to set the parameters for this simulation can be found in our work<sup>26</sup>. In the current modeling, the laminar flow module was utilised to solve the fluid flow in the three-dimensional model. No-slip boundary condition was set to the channel walls. The physical property of fluid was set to incompressible flow. The field flow inside the channel can be solved in the “Navier-Stokes Mode”. Stationary study was chose for the laminar flow module. The electric currents module was employed to calculate the non-uniform electric field generated by activated electrodes. A frequency solver was used to compute the electric field. Finally, the particle tracing module can couple DEP force and drag force to simulate the particle trajectories. The equation of DEP force has been described in the methodology section. The drag force is expressed as  $F_{drag} = -3\pi\eta d\mu$ . The dielectric properties for suspending medium and polystyrene beads are as followed:  $\epsilon_p = 2.55$ ,  $\sigma_p = 0$ ,  $\epsilon_m = 78.5$ ,  $\sigma_m = 0.0001 \text{ S/m}$ . Time-dependent study was performed to predict the particle trajectories. The time for beads migrating in the channel was set to 3 s and the interval time was set to  $10^{-4}$  s, which provided smooth particle trajectories. The simulation model was divided into 1,542,589 tetrahedrons. The particles injected into the channel have a diameter of 10  $\mu\text{m}$  and migrate under a flow rate of  $5 \mu\text{l min}^{-1}$ . Fig. 2a shows the movements of particles in the DEP-active hydrophoretic channel at a voltage of  $24 V_{p-p}$ . In the front section of the channel, particles were gradually levitated due to the negative DEP force induced by electrodes embedded at the bottom of the channel. Hydrophoretic ordering occurred to keep particles moving along the right sidewall of the channel. Particles flowed into the latter region following the spreading flow profile. However, particles could not enter the gap between microposts and right sidewall as their lateral position was larger than this gap (150  $\mu\text{m}$ ). At  $33 V_{p-p}$ , particles were pushed to higher positions in the channel. Thus, particles moved so close to the right sidewall that they could

pass through the gap and be collected from Outlet 2 (Fig. 2b). The lateral positions can be tuned by external electric field, which provides the opportunity to filter or separate particles.

### 2.3 Experimental details

Fluorescent micro-particles with diameters of 3, 5 and 10  $\mu\text{m}$  (Thermo Fisher Scientific., product number R0300, G0500 and G1000 and coefficient of variation 5%, 5% and 5%, respectively) were used in our experiments. They were prepared in deionized (DI) water, with 0.1% Tween 20 (Sigma-Aldrich, Product No. P9416) added to this particle suspension to stop the beads from sedimentation. The final concentration of beads for particle movement study was in the order of  $10^5$  beads per millilitre. For filtration and separation, the concentration of bead mixture was  $\sim 1 \times 10^6$  particles  $\text{ml}^{-1}$  and the concentration ratio of 3  $\mu\text{m}$  particles to 10  $\mu\text{m}$  particles was about 1:1. A mixture containing 5  $\mu\text{m}$  and 10  $\mu\text{m}$  beads were prepared for separation experiment with concentrations of  $\sim 560$  and  $420$  particles  $\mu\text{l}^{-1}$  for 5  $\mu\text{m}$  and 10  $\mu\text{m}$  beads.

The PDMS microfluidic channel was fabricated using a two-step photolithography technique. Detailed information for this fabrication technique can be found in our previous work<sup>26, 38, 39</sup>. Here a brief introduction is given. The first layer of photoresist (SU-8 2025, MicroChem Co., Newton, MA) was spun on the silicon wafer with a height of 35  $\mu\text{m}$ . After exposure and baking, the second layer with the pattern of grooves was fabricated using the same procedure and the pattern was aligned with the structures in the first layer. After the double-layer mold was developed, it was then treated by trichlorosilane to deposit a monolayer of silane on the surface for the ease of PDMS release. Sylgard 184 elastomer base and curing agent (Dow Corning Corporation, Midland, USA) were mixed evenly in a ratio of 10:1. The PDMS mixture was then poured onto the mold and then totally degassed under a vacuum chamber. After baking, the PDMS replica was peeled off the silicon wafer and inlet and outlet holes were punched with the tip of a custom made needle. After treating the flow layer and control layer with plasma (PDC-002, Harrick Plasma, Ossining, NY) for 3 min, the hydrophoretic channel was sealed with a glass slide patterned with interdigitated electrodes (see Supplementary information Fig. 1).

The dimensions of the interdigitated electrodes and microfluidic channel are described below. The spacing and the width of the electrodes were both 20  $\mu\text{m}$  (Fig. 1). The front region of hydrophoretic channel consisted of a series of grooves with a small curvature of 600  $\mu\text{m}$  and a large curvature of 650  $\mu\text{m}$ . The width of the latter section was  $W_2=800$   $\mu\text{m}$ , while the width of the front section was  $W_1=200$   $\mu\text{m}$  wide and its length was 10 mm. The gap between the microposts and right sidewall of the channel was  $W_3=150$   $\mu\text{m}$ .

The experiments were conducted on the stage of an inverted microscope (CKX41, Olympus, Japan). Distilled (DI) water with 0.1% Tween 20 was injected into the channel using a syringe pump (Legato 100, KD Scientific, Holliston, MA) to ensure that the polystyrene particles would not attach to PDMS surfaces during the experiment. The microfluidic channel was afterwards filled with air-bubble free particle suspension. During experiments, the flow rate of particle suspension was maintained at  $5 \mu\text{l min}^{-1}$  using a syringe pump (Legato 100, KD Scientific, Holliston, MA). A sinusoidal AC signal with frequency 1

MHz was generated by a waveform generator (33250A, Agilent, USA) and then amplified by an RF power amplifier (TIA-1000-1R8-2, Mini-Circuits, USA). The sliver wires soldered onto the pads were connected to the power amplifier to activate the electrodes. The images of fluorescent particles were recorded through a fluorescent filter and a 4× objective with a CCD camera (Rolera Bolt, Q-imaging, Australia). Q-Capture Pro 7 (Q-imaging, Australia), was used to post-process images. Particle samples collected from Outlet1 and 2 were analysed using a haemocytometer to quantitatively evaluate the separation efficiency and filtration performance.

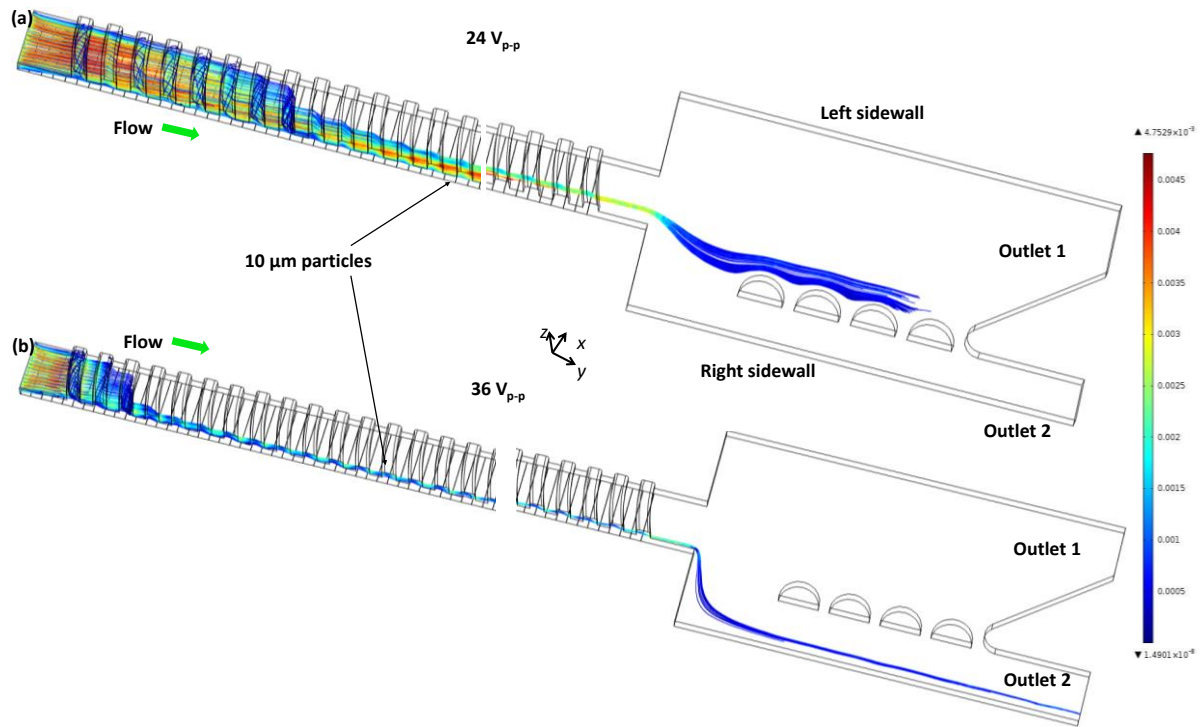


Figure 2 (a) Simulated trajectories of 10  $\mu\text{m}$  particles in the microchannel under 24  $V_{p-p}$ . The left image shows the entrance section and right the exit section. The color of the trajectories denotes particle velocity. Red means high speed and blue means low speed. The flow rate was  $5 \mu\text{l min}^{-1}$  and the flow direction was along the y-axis. (b) The images showing that particles moved along the right sidewall and were collected from outlet 2 under 33  $V_{p-p}$ . The scale bar illustrates the magnitude of the complete range of velocities.

### 3 Results and discussion

#### 3.1 Movements of 10 $\mu\text{m}$ particles

Since the working modes are determined to the movements of the large beads in the microfluidic channel, the conditions of focusing 10  $\mu\text{m}$  particles are first studied. The effect of voltage on the focusing positions of 10  $\mu\text{m}$  fluorescent particles is shown in Fig. 3. The particles with a diameter of 10  $\mu\text{m}$  were injected into the microchip and distributed themselves evenly at the inlet as the voltages varied from 24 to 39  $V_{p-p}$ . Fig. 3a shows trajectories of particles along the whole channel, which agree reasonably well with the simulation result shown in Fig. 2a. Beads forming the hydrophoretic ordering were focused along the right sidewall of the channel. Fig. 3b shows the optical micrographs of particle trajectories of 10  $\mu\text{m}$  particles passing the gap under various voltages.

Whether the beads go through the gap between microposts and right sidewall or not is dependent on their lateral positions. Choi and Park<sup>40</sup> reported that the lateral positions of the beads decreased when the height of the channel was lowered. Actually, applying a higher voltage can be the equivalent of reducing the channel height as the particles are pushed into a narrower space and can only migrate in the restricted area. That is, particles move closer to the sidewall of the channel with the increase of voltages. At the voltage of 33  $V_{p-p}$  or above, all 10  $\mu\text{m}$  particles passed through the gap between microposts and right sidewall, whereas they could not pass through at relatively low voltage. Once 10  $\mu\text{m}$  particles entered the area of Outlet 2, they were unable to pass through the gap between microposts as the particle diameter was larger than the minimum space between microposts (8  $\mu\text{m}$ ). Also, 10  $\mu\text{m}$  particles could not move from the area of Outlet 1 to Outlet 2 with the same principle. Therefore, the microposts embedded in the microchannel can significantly improve the separation and filtration performance.

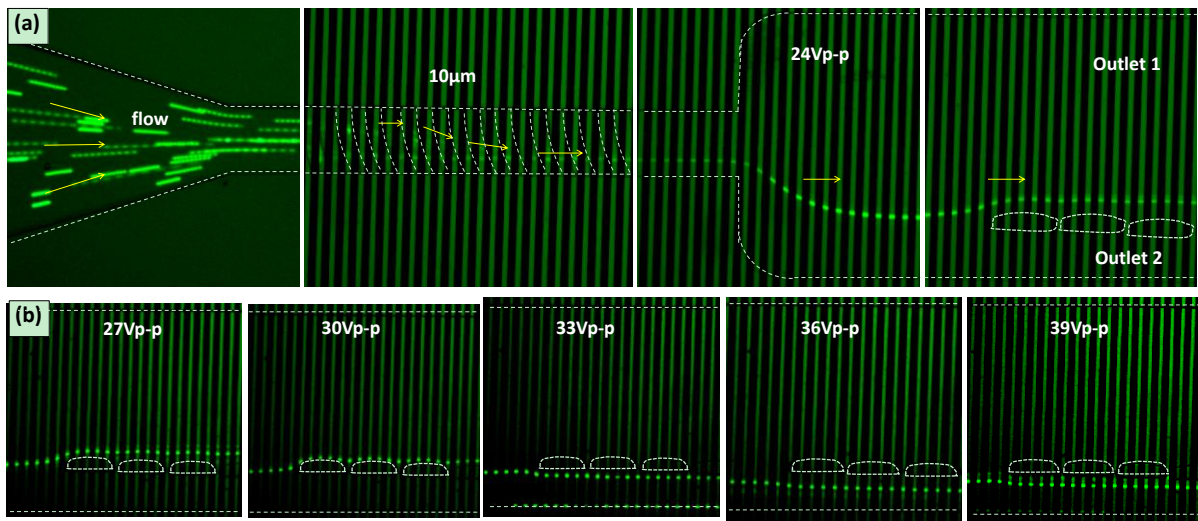


Figure 3 (a) Optical micrographs showing the trajectories of 10  $\mu\text{m}$  beads in the whole channel. The applied voltage was 24  $V_{p-p}$  and the applied flow rate was 5  $\mu\text{l min}^{-1}$ . (b) Fluorescence images showing the trajectories of 10  $\mu\text{m}$  beads in the latter section with voltages of 27, 30, 33, 36, 39  $V_{p-p}$ , separately.

### 3.2 Movements of 3 $\mu\text{m}$ particles

To investigate the capability of this microchip for simultaneously manipulating beads with different sizes, the particle trajectories of 3  $\mu\text{m}$  particles were tested under the same conditions as that of 10  $\mu\text{m}$  particles (Fig. 4). The optical micrographs in Fig. 4a show that the particles assumed a hydrophoretic ordering and focused themselves onto the right sidewall of the channel under the voltage of 24  $V_{p-p}$ . Fig. 4b shows the particle trajectories in the latter part of the channel with the voltage ranging from 27 to 39  $V_{p-p}$ .

The voltage had little effect on the lateral positions of 3  $\mu\text{m}$  particles which means that the higher voltages were unable to push the small particles to higher equilibrium position in the  $z$ -direction. Since the DEP force on the particle is proportional to the cube of their diameter, 3  $\mu\text{m}$  particles experience weaker DEP forces. Additionally, DEP force decreases exponentially with increasing the distance above the electrodes. Based on above reasons, the DEP force was insufficient to push particles to higher position in the channel. Therefore,

lateral positions of 3  $\mu\text{m}$  particles changed little under the voltage from 24 to 39  $V_{p-p}$ . Because the hydrodynamic resistance at Outlet 1 was larger than that at Outlet 2 due to the special design, beads with a diameter of 3  $\mu\text{m}$  would not pass through the gaps between microposts and tend to go out from Outlet 1.

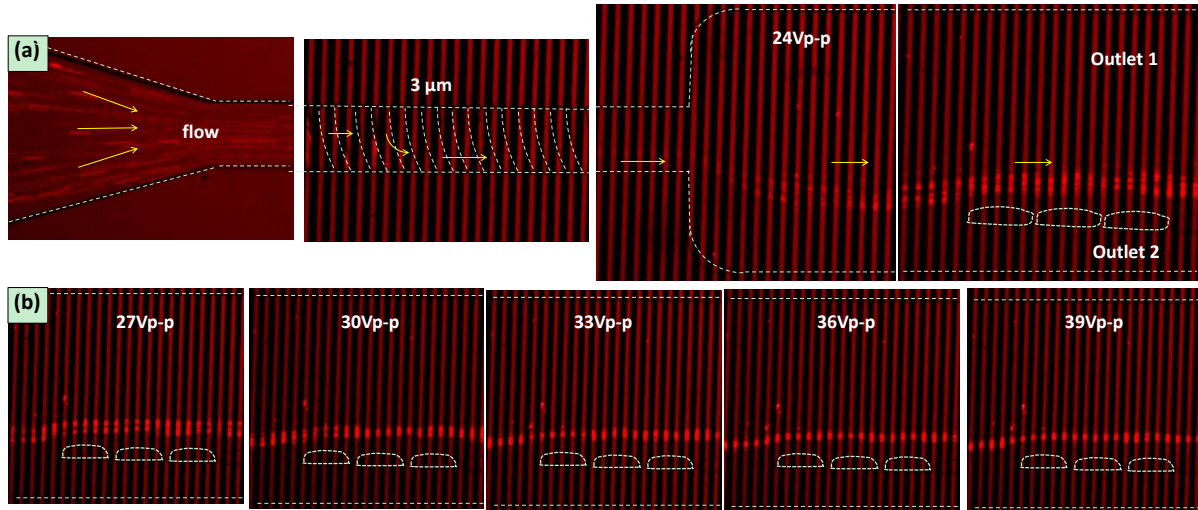


Figure 4 (a) Optical micrographs showing the trajectories of 3  $\mu\text{m}$  beads in the whole channel. The applied voltage was 24  $V_{p-p}$  and the applied flow rate was 5  $\mu\text{l min}^{-1}$ . (b) Fluorescence images showing the trajectories of 3  $\mu\text{m}$  beads in the latter section with voltages of 27, 30, 33, 36, 39  $V_{p-p}$ , separately.

### 3.3 Filtration of particles

Filtration was conducted with 3  $\mu\text{m}$  diameter (red) and 10  $\mu\text{m}$  diameter (green) fluorescent particles based on the particle trajectories under different working conditions in the previous sections. The mixture of 3  $\mu\text{m}$  and 10  $\mu\text{m}$  particles was introduced into the micro-channel with a voltage of 24  $V_{p-p}$ . Similar patterns were obtained from different particles, except for the focusing positions. 3  $\mu\text{m}$  and 10  $\mu\text{m}$  particles could not pass through the gap between micro-posts and right sidewall and were collected from Outlet 1 (Fig. 5a). As a result, the fluid through the Outlet 2 contains very little micro-particles. Fig. 5b and c show the fluorescent images of beads collected from inlet and Outlet 2. The current experiment showed that, after filtration, 99.0%  $\pm 0.3\%$  ( $n=3$ ) of 3  $\mu\text{m}$  beads and 100% ( $n=3$ ) of 10  $\mu\text{m}$  beads were filtered from initial particle-laden fluid solution.

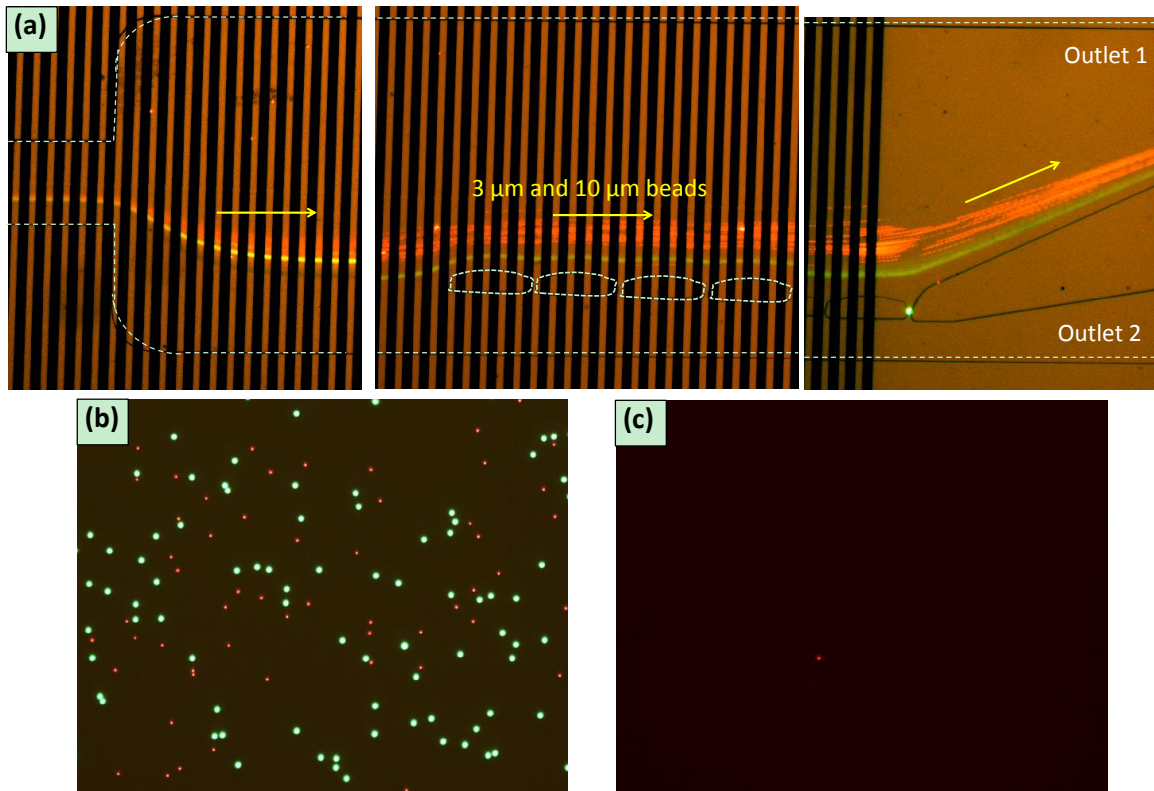


Figure 5 Filtration of 3  $\mu\text{m}$  and 10  $\mu\text{m}$  beads. The applied flow rate was  $5 \mu\text{l min}^{-1}$  and external voltage was  $24 V_{p-p}$ . The beads were evenly injected into the micro-channel. (a) Optical microscopy images showing the trajectories of 3  $\mu\text{m}$  and 10  $\mu\text{m}$  particles. The particles before (b) and after (c) filtration were illustrated in fluorescent images. These images were capture with  $50\times$  magnification.

### 3.4 Separation of particles

Once the applied voltage is over  $33 V_{p-p}$ , beads having 10  $\mu\text{m}$  in diameter pass through the gap between the microposts and right sidewall of the channel whereas 3  $\mu\text{m}$  beads cannot. As a result, fluid containing 3  $\mu\text{m}$  beads was collected from Outlet 1, while 10  $\mu\text{m}$  beads go through the Outlet 2. The separation experiment was conducted at a voltage of  $36 V_{p-p}$  and the results are shown in Fig. 6 a, b and c. As shown in Fig. 6a, the two size particles were completely separated. To quantify the separation performance, particle purity (collected target particle number/collected total number<sup>41</sup>) and separation efficiency (collected target particle number/input target particle number<sup>42</sup>) were measured. Fig. 6b and c show the fluorescent images of beads collected from Outlet 1 and Outlet 2, respectively. After sorting, the 10  $\mu\text{m}$  beads were collected from Outlet 2 with a separation efficiency of 100% and a purity of  $98.6 \pm 0.8\%$ , whereas for the 3  $\mu\text{m}$  particles, a separation efficiency of  $99.4 \pm 0.2\%$  and a purity of 100% were recovered from Outlet 1. To demonstrate the capability of our device that can separate other particle sizes, a mixture of 5 and 10  $\mu\text{m}$  particles was introduced into the microchannel at a voltage of  $39 V_{p-p}$  (Fig. 6d). Although increasing the voltage could not change the lateral positions of 5  $\mu\text{m}$  particles a lot, a higher voltage enabled small particles (5  $\mu\text{m}$  particles) focus well in the latter section of the channel. Therefore, the separation of 5 and 10  $\mu\text{m}$  particles was performed at  $39 V_{p-p}$ . Fig. 6e and f show the separated beads collected from Outlet 1 and Outlet 2, respectively. By the

separation process, 5  $\mu\text{m}$  particles were separated at the Outlet 1 with a purity of  $96.6\% \pm 1.2\%$ . The separation efficiency for 5  $\mu\text{m}$  was  $98.5 \pm 0.5\%$ . A particle population was collected from the Outlet 2 that held  $90.9 \pm 2.3\%$  10  $\mu\text{m}$  particles. Up to  $86.2 \pm 3.0\%$  of 10  $\mu\text{m}$  particles were separated from their initial particle suspending.

High separation performance was achieved because polystyrene particles with different size were pre-separated after entering the latter section of the channel. Both small and large particles were well focused in the front section of the device at  $36 V_{p-p}$  and their equilibrium positions were slightly different with each other (See supplementary information Fig. 2). The relative distance between these two trajectories can be further enlarged after entering the latter section due to the spreading flow profile at the junction of the front and latter section. Then, the microposts served as a re-purifying unit to remove the unseparated small particles from Outlet 2<sup>43</sup>. The special design makes the hydrodynamic resistance of Outlet 1 higher than that of Outlet 2. This mismatched pressure allowed a small amount of liquid to be withdrawn through the spaces between microposts to Outlet 1, which brought a small amount of the unseparated small particles into the Outlet 1. Therefore, the particles were separated with high separation efficiency and purity. Additionally, this device has the potential to separate three or more different size particles as the lateral positions of beads in the channel are size-dependent.

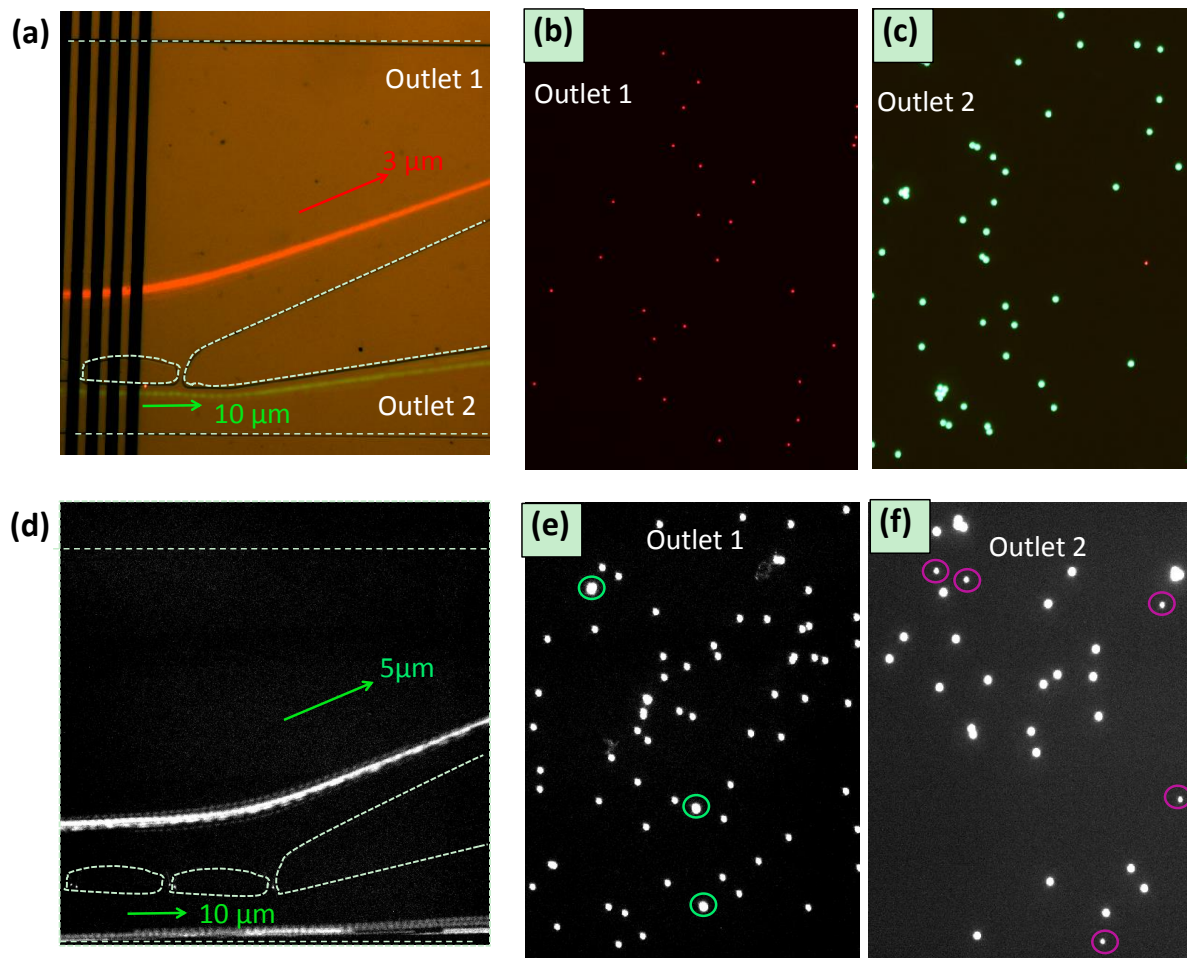


Figure 6 (a) Separation of 3  $\mu\text{m}$  and 10  $\mu\text{m}$  beads. The applied flow rate was  $5 \mu\text{l min}^{-1}$  and external voltage was  $36 V_{p-p}$ . The beads were evenly injected into the micro-channel. Optical micrographs showing the trajectories of 3 and 10  $\mu\text{m}$  beads after entering the latter section. Beads collected from outlet 1 (b) and outlet 2 (c) were shown

in fluorescence images. (d) Micro-image showing the separation of 5  $\mu\text{m}$  and 10  $\mu\text{m}$  beads. The applied flow rate was 5  $\mu\text{l min}^{-1}$  and external voltage was 39  $V_{\text{p-p}}$ . Beads collected from outlet 1 (e) and outlet 2 (f) were shown in fluorescence images. These images were capture with 50 $\times$  magnification.

#### 4 Conclusions

An integrated DEP-active hydrophoretic device has been developed in this study for particle separation and filtration. A mixture of 3 and 10  $\mu\text{m}$  polystyrene particles were used to test the performance of this device. Both 3  $\mu\text{m}$  and 10  $\mu\text{m}$  beads can be filtered from particle suspending in the filtration mode, while they can be separated by the micro-posts embedded in the microchannel in the separation mode. In filtration mode, 99.0%  $\pm$ 0.3% of 3  $\mu\text{m}$  beads and 100% of 10  $\mu\text{m}$  beads were filtered from initial particle-laden fluid solution. In separation mode, the 10  $\mu\text{m}$  beads were collected from Outlet 2 with a separation efficiency of 100% and a purity of 98.6  $\pm$  0.8%, whereas for the 3  $\mu\text{m}$  particles, a separation efficiency of 99.4  $\pm$  0.2 % and a purity of 100% were recovered from Outlet 1. A mixture of 5 and 10  $\mu\text{m}$  particles was well separated in this integrated device, which proved that the relatively small size difference of the particles can be separated readily. This integrated microfluidic device has practical potential to a critical component in advanced lab-on-a-chip devices, which could be utilised for sample preparation and clinical diagnosis.

#### Acknowledgements

This work is supported by the University of Wollongong -China Scholarship Council joint scholarships and the CSIRO Office of Chief Executive (OCE) Top-up Scholarship.

1. G. M. Whitesides, *Nature*, 2006, **442**, 368-373.
2. P. Sajeesh and A. K. Sen, *Microfluid. Nanofluid.*, 2013, 1-52.
3. J. Zhang, S. Yan, G. Alici, N.-T. Nguyen, D. Di Carlo and W. Li, *RSC Advances*, 2014, **4**, 62076-62085.
4. I. F. Cheng, H.-C. Chang, D. Hou and H.-C. Chang, *Biomicrofluid.*, 2007, **1**.
5. J. Shi, X. Mao, D. Ahmed, A. Colletti and T. J. Huang, *Lab Chip*, 2008, **8**, 221-223.
6. C. Liu, T. Stakenborg, S. Peeters and L. Lagae, *J. Appl. Phys.*, 2009, **105**.
7. B. Cetin and D. Li, *Electrophoresis*, 2011, **32**, 2410-2427.
8. V. Chaurey, C. Polanco, C.-F. Chou and N. S. Swami, *Biomicrofluid.*, 2012, **6**, 12806-1280614.
9. M. Li, S. Li, W. Cao, W. Li, W. Wen and G. Alici, *J. Micromech. Microeng.*, 2012, **22**.
10. M. Yamada, M. Nakashima and M. Seki, *Anal. Chem.*, 2004, **76**, 5465-5471.
11. L. R. Huang, E. C. Cox, R. H. Austin and J. C. Sturm, *Science*, 2004, **304**, 987-990.
12. J. McGrath, M. Jimenez and H. Bridle, *Lab Chip*, 2014, **14**, 4139-4158.
13. S. Choi, S. Song, C. Choi and J.-K. Park, *Lab Chip*, 2007, **7**, 1532-1538.
14. S. Choi, S. Song, C. Choi and J. K. Park, *Small*, 2008, **4**, 634-641.
15. S. Song and S. Choi, *J. Chromatogr. A*, 2013, **1302**, 191-196.
16. D. Di Carlo, *Lab Chip*, 2009, **9**, 3038-3046.
17. J. Zhang, S. Yan, R. Sluyter, W. Li, G. Alici and N.-T. Nguyen, *Sci. Rep.*, 2014, **4**.
18. J. Zhang, W. Li, M. Li, G. Alici and N. T. Nguyen, *Microfluid. Nanofluid.*, 2013, 1-12.
19. R. C. Gallo-Villanueva, V. H. Pérez-González, R. V. Davalos and B. H. Lapizco-Encinas, *Electrophoresis*, 2011, **32**, 2456-2465.
20. J. P. Beech, P. Jonsson and J. O. Tegenfeldt, *Lab Chip*, 2009, **9**, 2698-2706.
21. S. Park, Y. Zhang, T. H. Wang and S. Yang, *Lab Chip*, 2011, **11**, 2893-2900.
22. N. Lewpiriyawong, C. Yang and Y. C. Lam, *Electrophoresis*, 2010, **31**, 2622-2631.
23. H. Song, J. M. Rosano, Y. Wang, C. J. Garson, B. Prabhakarpanthian, K. Pant, G. J. Klarmann, A. Perantoni, L. M. Alvarez and E. Lai, *Lab Chip*, 2015, **15**, 1320-1328.
24. Z. Wu, A. Q. Liu and K. Hjort, *J. Micromech. Microeng.*, 2007, **17**, 1992-1999.
25. S. Yan, J. Zhang, M. Li, G. Alici, H. Du, R. Sluyter and W. Li, *Sci. Rep.*, 2014, **4**, 5060.
26. S. Yan, J. Zhang, G. Alici, H. Du, Y. Zhu and W. Li, *Lab Chip*, 2014, **14**, 2993-3003.
27. S. Yan, J. Zhang, Y. Yuan, G. Lovrecz, G. Alici, H. Du, Y. Zhu and W. Li, *Electrophoresis*, 2014, n/a-n/a.
28. C. Li, C. Liu, Z. Xu and J. Li, *Talanta*, 2012, **97**, 376-381.
29. K. H. Chung, Y. H. Choi, J.-H. Yang, C. W. Park, W.-J. Kim, C. S. Ah and G. Y. Sung, *Lab Chip*, 2012, **12**, 3272-3276.
30. K. Aran, A. Fok, L. A. Sasso, N. Kamdar, Y. Guan, Q. Sun, A. Undar and J. D. Zahn, *Lab Chip*, 2011, **11**, 2858-2868.
31. D. Gossett, W. Weaver, A. Mach, S. Hur, H. Tse, W. Lee, H. Amimi and D. Di Carlo, *Anal. Bioanal. Chem.*, 2010, **397**, 3249-3267.
32. T. B. Jones, *Electromechanics of Particles*, Cambridge University Press, Cambridge, 1995.
33. S. Choi, *Anal. Chem.*, 2009, **81**, 50-55.
34. J. Han, J. Fu and R. B. Schoch, *Lab Chip*, 2007, **8**, 23-33.
35. S. Song and S. Choi, *Appl. Phys. Lett.*, 2014, **104**, 074106.
36. S. Song, M. S. Kim, J. Lee and S. Choi, *Lab Chip*, 2015, **15**, 1250-1254.
37. J. J. Agresti, E. Antipov, A. R. Abate, K. Ahn, A. C. Rowat, J.-C. Baret, M. Marquez, A. M. Klibanov, A. D. Griffiths and D. A. Weitz, *Proc. Natl. Acad. Sci. U.S.A.*, 2010, **107**, 4004-4009.
38. J. Zhang, M. Li, W. H. Li and G. Alici, *J. Micromech. Microeng.*, 2013, **23**.

39. M. Li, S. Li, J. Wu, W. Wen, W. Li and G. Alici, *Microfluid. Nanofluid.*, 2012, **12**, 751-760.
40. S. Choi and J.-K. Park, *Lab Chip*, 2007, **7**, 890-897.
41. J. Zhou, P. V. Giridhar, S. Kasper and I. Papautsky, *Lab Chip*, 2013, **13**, 1919-1929.
42. K. Louthback, J. D'Silva, L. Liu, A. Wu, R. H. Austin and J. C. Sturm, *AIP Advances*, 2012, **2**.
43. S. Shen, C. Ma, L. Zhao, Y. Wang, J.-C. Wang, J. Xu, T. Li, L. Pang and J. Wang, *Lab Chip*, 2014.